5. CHARACTERIZATION OF LOW AND HIGH MOLECULAR-WEIGHT HYDROCARBONS IN SEDIMENTS FROM THE BLAKE RIDGE, SITES 994, 995, AND 997[1]

Hermann Wehner,[2] Eckhard Faber,[2] and Heinz Hufnagel[2]

ABSTRACT

Sediments from Holes 994C, 995A, 997A, and 997B have been investigated for "combined" gases (adsorbed gas and that portion of free gas that has not escaped from the pore volume during core recovery and sample collection and storage), solvent-extractable organic compounds, and microscopically identifiable organic matter. The soluble materials mainly consist of polar compounds. The saturated hydrocarbons are dominated by *n*-alkanes with a pronounced odd-even predominance pattern that is derived from higher plant remains. Unsaturated triterpenoids and 17ß, 21ß-pentacyclic triterpenoids are characteristic for a low maturity stage of the organic matter. The low maturity is confirmed by vitrinite reflectance values of 0.3%. The proportion of terrestrial remains (vitrinite) increases with sub-bottom depth. Within the liptinite fraction, marine algae plays a major role in the sections below 180 mbsf, whereas above this depth sporinites and pollen from conifers are dominant. These facies changes are confirmed by the downhole variations of isoprenoid and triterpenoid ratios in the soluble organic matter.

The combined gases contain methane, ethane, and propane, which is a mixture of microbial methane and thermal hydrocarbon gases. The variations in the gas ratios $C_1/(C_2+C_3)$ reflect the depth range of the hydrate stability zone. The carbon isotopic contents of ethane and propane indicate an origin from marine organic matter that is in the maturity stage of the oil window.

INTRODUCTION

The sites of Leg 164 were all drilled at the eastern end of the Blake Ridge and southernmost Carolina Continental Rise. Previous investigations of Deep Sea Drilling Project (DSDP) Sites 102, 103, 104 (Shipboard Scientific Party, 1972), and 533 (Sheridan, Gradstein, et al., 1983) revealed that the Blake Ridge is a major Neogene and Quaternary sediment drift that consists of hemipelagic silt- and clay-rich contourite deposits. The objectives of Leg 164 were to increase the understanding of all the aspects of generation and occurrence of gas hydrates and their impact on the environment in an area where their existence had already been suggested by observations on DSDP Leg 11 (Claypool et al., 1973) and verified by sampling on DSDP Leg 76 (Kvenvolden and Barnard, 1983).

We have characterized the amount and composition of the organic matter in the drilled sections to explain its possible contribution to the formation of gas hydrates. The investigations were conducted on whole-round cores from Holes 994C, 995A, 997A, and 997B. One of the targets was to look for the occurrence of thermogenic gases. Only the deep holes of Leg 164 were sampled to determine the extent of in situ formation of gases during maturation of the sedimentary organic matter with increasing depth.

Sites 994, 995, and 997 make up a transect of holes that have penetrated below the base of gas hydrate stability within the same stratigraphic interval over a short distance of 9.6 km. Even within this distance, small variations in the composition of the organic matter (Rock-Eval data, maceral data) occurred. The ages of the sediments drilled at the three locations are roughly the same and in the range of late Miocene to Pleistocene

Three lithostratigraphic units were identified in all three holes based on sediment composition and primary variations in the nannofossil and total carbonate contents. The sediments consist mostly of green to gray nannofossil-bearing clays, claystones, and marls of late

Miocene to Holocene age (Paull, Matsumoto, Wallace, et al., 1996). Pyrite is a common accessory mineral and occurs throughout the profile, being somewhat less abundant in deeper sections. Microfossils (diatoms, foraminifer, sponge spicules, and chitinous-phosphatic faunal relics) constitute the coarsest fraction of the sediments.

TECHNIQUES

After the cores were recovered, they were cut into sections at the catwalk, and the sediment samples within the plastic liners were deep frozen in liquid nitrogen immediately. Unfortunately, the cooling chain was interrupted during transport to Germany. For this reason the samples reached temperatures above zero for a few days. They were kept in a deep freezer (at ~–20°C) again until the laboratory investigation commenced. For the analysis of the nonvolatile organic matter, the samples were freeze dried and aliquots were impregnated with a resin for organic petrographic investigations. After having polished the blocks, maceral composition and vitrinite reflectance were measured under the microscope using incident light of 546 nm and fluorescence illumination with blue light irradiation. Due to the scarcity and the small size of the huminite only 2–14 readings per sample were achieved.

The composition of the structured organic matter is determined by a semiquantitative estimation method that is based on a procedure applied successfully for vegetation surveys (Hufnagel and Porth, 1989). The contents of the main components (liptinite, bituminite, vitrinite, inertinite, and fecal pellets) are given in percent, and the composition of the liptinite (sporinite, alginite, and faunal liptinite) is similarly expressed. For organic-geochemical analysis, the dried samples were crushed in a disc mill. Total carbon and sulfur content were analyzed in the untreated sample with a LECO CS-444 analyzer. Prior to total organic carbon (TOC) analyses and the determination of $^{13}C/^{12}C$ ratios of kerogens, carbonate carbon was removed with hot 2N HCl (80ºC, 3 hr). Calibration was done with LECO steel rings and a homemade rock standard. The error associated with the TOC analysis is ±3% relative.

The crushed samples were extracted for 3.5 hr in a Soxtec device with acetone/hexane (50:50, v:v) as solvent, along with activated

copper granules as a sulfur-removing agent. Due to the low amounts of soluble organic matter obtained, no further separation by quantitative liquid chromatography was done. After precipitation of the asphaltenes with *n*-pentane, the remainder was cleaned up by filtering it over aluminum oxide. Gas chromatographic separation of the nonaromatic fractions was done on a 30 m DB 5 fused silica column in a Hewlett Packard (HP) 5890 gas chromatograph connected to a HP 5972 mass selective detector (MSD). For the identification of normal- and cyclo-alkanes, mass spectra and retention times were used.

Extraction of hydrocarbon gases from the wet samples was done with a vacuum-degassing system (similar to that described by Faber and Stahl, 1983). About 150 g of sample material was heated to 100ºC in a closed bulb (~1 L), and phosphoric acid was added through a valve. The "combined" gases were extracted from the unsieved samples, consisting of "free" and "sorbed" hydrocarbon gases (e.g., Faber et al., 1990). Free gases are considered to consist predominantly of bacterial methane, thermal gases are mainly found in the sorbed phase, and combined gases are often a mixture of bacterial methane and thermal hydrocarbon gases (Faber et al., 1997, Whiticar and Suess, 1990).

Gas concentrations are measured using a conventional gas chromatograph. Data is given in parts per billion by weight (ppbw). Gas ratios (e.g., $C_1/[C_2+C_3]$) are based on volumetric concentrations. For isotope analyses, methane (C_1), ethane (C_2), and propane (C_3) are separated on a GC column and oxidized to CO_2 and H_2O. The CO_2 is used for stable carbon isotope ratio determination with an isotope-ratio mass spectrometer (Finnigan MAT 251 IR-MS). The isotope ratios are given in the δ-notation and are related to the Peedee belemnite (PDB) standard. The standard deviations of the isotope values for the sediment gases are in the order of ± 1‰ for $\delta^{13}C_1$, $\delta^{13}C_2$, and $\delta^{13}C_3$ (see Dumke et al., 1989). Minimum sample quantities are about 1 μL for $\delta^{13}C_1$, $\delta^{13}C_2$, and $\delta^{13}C_3$. Deuterium measurements could not be performed due to the insufficient gas quantity.

RESULTS

Amount and Composition of the Solvent-Extractable Organic Matter and the Kerogen

The TOC contents of the samples from all three holes increase from 0.3% to 0.5% in the uppermost samples to levels around 1.5% at a depth of about 200 mbsf, and remain constant below (Fig. 1; Table 1). Shipboard and shore-based results correlate despite the fact that quite different methods were used (Shipboard Scientific Party, 1996). The total sulfur contents (TS) are around 1% for all samples. No correlation between the TOC content and the TS nor a depth trend in the TS concentrations was observed. Only samples from within the sulfate-reduction zone appear to be depleted in sulfur.

Between 100 and 1000 ppm soluble organic matter (SOM) could be extracted from the dried sediments. There is a weak but nonlinear correlation to the TOC concentration. Normalized to the TOC content 1%–6% of the organic carbon is soluble with a slight tendency towards an increasing solubility with increasing TOC contents. However, an increase of the SOM/TOC ratio (ratio is not expressed in Table 1) with depth that would indicate a maturation effect is absent.

A large part of the extract consists of asphaltenes (up to 22%) and other polar compounds. The nonaromatic hydrocarbon fraction comprises normal-, iso-, and cyclo-alkanes and alkenes. The *n*-alkanes contain from 16 to 35 C atoms with a pronounced odd-even-predominance in the high boiling range. The alkane n-$C_{29}H_{60}$ is typically the most prominent compound in the chromatograms, which indicates a contribution of higher land plants to the organic matter (Eglinton and Hamilton, 1963), although odd-numbered long-chain *n*-alkanes have been detected also in various species of microalgae (Zegouagh et al., 1998). About 40% of the samples are characterized by *n*-alkane distribution curves that show a second maximum around n-$C_{17}H_{36}$,
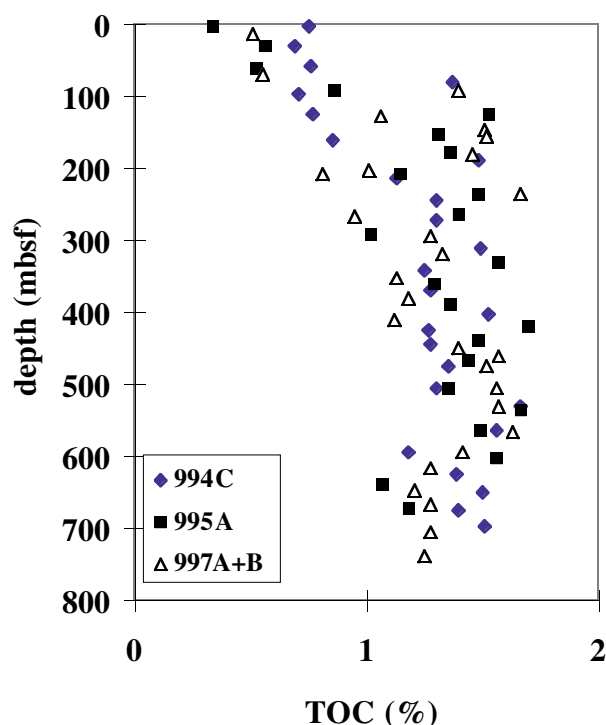
Figure 1. Total organic carbon (TOC) vs. depth for Holes 994C, 995A, 997A, and 997B.

which unequivocally suggests an algal input (Fig. 2A; Blumer et al., 1971). These samples are more concentrated in the Pleistocene–Pliocene part of the profiles. The changes in the relative composition of the organic matter with increasing age of the sediments is expressed by the change in a variety of hydrocarbon ratios (Fig. 3; Table 1).

1. The concentration of the isoprenoids pristane and phytane relative to n-$C_{17}H_{36}$ and n-$C_{18}H_{38}$ is constant with depth until about 400 m. At the final depth, pristane/n–$C_{17}H_{36}$ ratios as high as 2 and phytane/n-$C_{18}H_{38}$ ratios as high as about 6 were determined, whereas these ratios are below 1 in the near-surface samples (Figs. 3A, 3B).

2. The pristane/phytane concentration ratios decrease from levels around 1 at the sediment surface to about 0.3 at the final depth in all three boreholes (Fig. 3C).

3. All samples contain thermally unstable hopenes and ß, ß-hopanes in varying amounts (Figs. 2C, 2D; Table 2; Figs. 3D, 3F), which indicates the immature stage of the sediments. The concentration of these compounds, relative to that of the stable α,ß-hopanes, increases with depth, which shows that maturation does not play a major role in transforming the organic matter. Otherwise the depth trend of the ratios plotted in Figures 3D and 3F should be reversed.

4. The odd-even-predominance (calculated for the n-$C_{27}H_{56}$) increases steadily from around 1 to 2 at the seabed to ratios of around 3.6 and 3.0 at the final depths of Holes 994C and 995A, whereas it is rather constant at about 2 for the profile of Holes 997A and 997B (Fig. 3E). Again, if maturation would have been the dominating factor, an opposite depth trend for Holes 994C and 995A should occur.

Aside from the features of immaturity present in all samples (odd-even predominance of *n*-alkanes, unstable hopenes and hopanes),

Table 1. Organic-geochemical data of samples from Holes 994C, 995A, 997A, and 997B.

Core, section	Age	Depth (mbsf)	C (tot) (%)	C (carb) (%)	TOC (%)	TS (%)	Sol (ppm)	Pri C17	Phy C18	Pri	OEP 27	hop17 hopane	ß,ß-hop hopane	δ13C kerogen
164-994C-														
1H-2	Pleistocene	2.95	2.41	1.66	0.75	0.46	243	0.48	0.56	0.54	1.18	0.01	0.50	ND
4H-4	Pleistocene	29.35	3.33	2.64	0.69	0.89	366	0.59	0.69	1.30	1.60	0.10	1.00	ND
7H-5	Pleistocene	59.35	2.05	1.29	0.76	0.91	386	0.56	0.81	0.77	2.42	0.26	1.19	ND
10H-5	Pleistocene	79.35	4.30	2.93	1.37	0.74	516	0.45	0.41	1.00	2.75	0.24	2.09	ND
12H-5	Pleistocene	98.35	2.42	1.71	0.71	0.85	431	0.45	0.40	0.95	2.54	0.29	1.62	ND
15H-5	Pliocene	126.13	3.41	2.64	0.77	1.27	240	0.50	0.55	0.70	2.22	0.34	1.73	ND
20X-1	Pliocene	159.85	2.42	1.57	0.85	2.20	325	0.46	0.49	0.51	2.27	0.12	1.59	ND
23X-4	Pliocene	189.95	2.53	1.05	1.48	1.37	352	0.62	0.64	0.78	2.46	0.29	1.96	ND
26X-1	Pliocene	214.35	2.46	1.33	1.13	1.01	506	0.69	0.69	0.58	2.94	0.37	1.86	ND
30X-1	Pliocene	243.15	3.20	1.90	1.30	1.16	318	0.40	0.50	0.54	2.69	0.21	1.72	ND
33X-2	Pliocene	273.24	3.92	2.62	1.30	1.04	452	0.40	0.59	0.55	3.21	0.56	2.30	ND
38X-1	Pliocene	310.40	3.60	2.11	1.49	1.09	466	0.27	2.47	0.08	1.44	0.68	1.71	ND
41X-2	Pliocene	340.40	3.11	1.86	1.25	1.43	365	0.76	0.70	0.29	2.27	0.57	1.03	ND
44X-2	Pliocene	369.60	2.81	1.53	1.28	1.08	572	0.60	0.70	0.63	2.68	0.78	1.56	ND
49X-5	Pliocene	402.62	3.76	2.23	1.53	0.64	165	0.71	0.55	0.32	2.09	0.92	1.71	ND
52X-1	Pliocene	425.95	3.72	2.45	1.27	1.00	470	0.67	1.66	0.28	3.00	1.18	2.18	ND
55X-1	Pliocene	444.76	2.92	1.64	1.28	1.18	383	0.75	1.11	0.39	2.97	0.59	0.93	ND
58X-1	Pliocene	473.90	2.92	1.57	1.35	1.13	335	0.84	1.12	0.25	2.58	1.93	2.24	ND
62X-2	late Miocene	504.30	3.09	1.79	1.30	1.23	816	0.61	1.04	0.50	2.70	1.15	1.72	ND
65X-5	late Miocene	529.50	3.13	1.47	1.66	0.96	505	1.25	2.97	0.34	3.10	1.69	2.65	ND
69X-3	late Miocene	563.66	3.02	1.46	1.56	0.99	324	2.72	5.24	0.34	3.65	1.48	2.62	ND
73X-4	late Miocene	593.07	2.31	1.13	1.18	0.87	415	0.77	1.11	0.32	3.10	1.31	2.22	ND
76X-5	late Miocene	624.30	3.37	1.98	1.39	0.18	523	0.65	1.35	0.42	3.03	1.68	2.26	ND
79X-4	late Miocene	650.71	3.52	2.02	1.50	0.84	541	1.12	2.91	0.24	3.63	1.72	3.14	ND
82X-1	late Miocene	676.05	3.18	1.78	1.40	1.14	360	0.76	1.48	0.36	3.37	1.31	2.11	ND
84X-2	late Miocene	696.45	3.28	1.77	1.51	0.99	555	0.70	1.17	0.57	3.31	1.66	2.37	ND
164-995A-														
2H-1	Pleistocene	3.15	2.35	2.01	0.34	0.12	92	0.46	0.41	0.52	1.95	0.22	1.09	−21.9
5H-1	Pleistocene	31.65	2.64	2.08	0.56	0.93	198	0.55	0.62	0.60	2.30	0.36	1.58	−20.9
8H-2	Pleistocene	61.65	1.68	1.15	0.53	1.42	271	0.80	0.85	0.79	1.98	0.23	1.03	−20.8
12H-3	Pleistocene	91.58	3.93	3.07	0.86	0.91	343	0.60	0.80	0.50	2.54	0.14	1.65	−20.7
15H-5	Pliocene	124.15	3.99	2.46	1.53	1.63	641	0.61	0.82	0.62	2.67	0.50	2.48	−21.3
19H-5	Pliocene	152.78	2.92	1.61	1.31	1.03	679	0.55	0.59	1.10	2.53	0.46	2.40	−20.9
22X-2	Pliocene	177.60	2.25	0.89	1.36	1.31	808	0.51	0.51	1.55	2.28	0.39	1.85	−20.5
25X-3	Pliocene	208.00	2.57	1.42	1.15	1.00	529	0.58	0.70	0.74	2.16	0.28	1.08	−20.5
29X-2	Pliocene	235.58	3.30	1.82	1.48	0.94	253	0.55	0.57	0.88	2.27	0.60	1.75	−20.9
32X-1	Pliocene	263.23	3.44	2.04	1.40	1.04	602	0.52	1.05	0.57	1.69	0.55	2.04	−20.6
35X-1	Pliocene	291.90	2.65	1.63	1.02	1.13	205	0.52	0.79	0.41	2.76	0.41	1.47	−20.5
40X-2	Pliocene	331.64	3.31	1.74	1.57	0.90	602	0.41	0.87	0.61	2.40	0.69	1.79	−21.4
43X-2	Pliocene	361.15	3.05	1.76	1.29	1.19	618	0.57	0.95	0.56	3.31	1.25	2.69	−20.7
47X-2	Pliocene	389.85	3.71	2.35	1.36	1.07	585	0.50	16.79	0.03	3.13	0.94	2.68	−20.6
51X-2	Pliocene	418.75	3.88	2.18	1.70	0.97	1052	0.42	0.65	0.94	2.92	1.53	2.11	−20.8
54X-3	Pliocene	439.60	3.88	2.40	1.48	0.83	810	0.69	1.59	0.54	2.57	1.41	2.71	−20.8
57X-2	Pliocene	467.10	3.38	1.94	1.44	0.95	650	0.74	2.76	0.24	2.81	1.31	2.46	−20.8
62X-3	Pliocene	506.56	3.18	1.83	1.35	1.22	796	0.72	0.37	1.99	3.51	1.97	2.45	−21.0
65X-3	Pliocene	536.00	3.66	2.00	1.66	1.13	898	1.13	3.09	0.38	2.88	2.42	3.34	−20.4
68X-2	late Miocene	563.30	3.03	1.54	1.49	0.93	750	1.02	2.76	0.50	2.78	1.71	2.78	−21.3
73X-4	late Miocene	603.99	3.55	1.99	1.56	0.90	853	1.94	5.47	0.38	2.78	1.72	2.59	−21.2
77X-3	late Miocene	640.27	3.51	2.44	1.07	0.85	237	1.79	4.42	0.53	2.98	1.73	2.38	−20.5
80X-4	late Miocene	671.42	2.87	1.69	1.18	1.12	413	0.78	1.79	0.25	3.06	1.33	2.35	−21.0
164-997A-														
3H-2	Pleistocene	15.25	2.50	1.99	0.51	0.67	197	0.49	0.61	0.75	2.59	ND	0.62	ND
9H-6	Pliocene	70.35	3.63	3.08	0.55	0.62	241	0.54	0.61	0.85	2.54	ND	1.17	ND
12H-2	Pliocene	92.70	3.78	2.38	1.40	1.58	562	0.50	0.61	0.87	2.63	0.55	2.45	ND
15H-6	Pliocene	127.35	2.86	1.80	1.06	1.31	405	0.52	0.59	0.86	5.37	0.41	2.05	ND
18P-1	Pliocene	146.90	3.24	1.73	1.51	1.42	794	0.53	0.75	0.80	2.14	ND	0.36	ND
19H-5	Pliocene	154.63	2.73	1.21	1.52	1.45	614	0.42	0.56	0.79	2.32	0.43	2.08	ND
22X-5	Pliocene	179.54	2.42	0.96	1.46	0.98	1048	0.44	0.44	1.11	1.78	0.25	1.21	ND
25P-1	Pliocene	202.81	2.14	1.13	1.01	1.18	576	0.67	1.32	1.06	2.15	0.05	0.20	ND
26X-3	Pliocene	207.85	2.14	1.33	0.81	0.32	312	1.08	3.86	0.45	2.80	0.70	1.98	ND
30X-3	Pliocene	236.24	3.23	1.57	1.66	1.05	1044	0.46	0.56	1.06	7.57	0.57	1.66	ND
34X-4	Pliocene	266.78	2.34	1.39	0.95	1.44	360	0.48	0.54	0.72	2.24	0.58	1.62	ND
37X-4	Pliocene	294.85	3.33	2.05	1.28	1.02	551	0.52	0.52	0.65	2.91	0.99	2.48	ND
41X-1	Pliocene	320.10	3.51	2.18	1.33	0.92	383	0.47	0.52	0.72	3.60	1.05	2.45	ND
44X-4	Pliocene	352.60	2.79	1.66	1.13	1.07	501	0.47	0.67	0.80	2.17	0.67	1.66	ND
47X-3	Pliocene	379.67	3.60	2.42	1.18	1.00	323	0.52	0.82	0.25	2.26	0.68	1.67	ND
52X-4	Pliocene	411.20	3.28	2.16	1.12	1.17	459	0.59	0.64	0.52	2.70	0.90	2.40	ND
164-997B-														
8X-4	Pliocene	448.80	3.40	2.00	1.40	1.28	312	0.99	2.95	0.18	2.43	1.16	1.95	ND
10P-1	Pliocene	462.20	3.15	1.58	1.57	1.17	1017	1.39	3.25	0.49	1.91	0.08	0.18	ND
12X-3	late Miocene	475.56	3.64	2.12	1.52	1.04	689	0.88	2.81	0.49	1.06	0.81	1.48	ND
16X-3	late Miocene	506.25	3.33	1.77	1.56	1.05	739	1.25	4.13	0.24	2.99	1.41	2.61	ND
19X-1	late Miocene	531.00	3.19	1.62	1.57	0.93	269	1.16	2.89	0.31	2.36	1.01	2.13	ND
23X-6	late Miocene	567.35	3.26	1.63	1.63	0.95	765	1.94	5.76	0.39	2.69	1.43	2.66	ND
27X-5	late Miocene	594.70	2.91	1.50	1.41	0.10	589	0.97	2.33	0.35	1.74	1.38	2.32	ND
30X-1	late Miocene	617.50	3.25	1.97	1.28	1.02	648	0.98	3.19	0.45	1.59	1.13	1.53	ND
34X-1	late Miocene	646.40	2.25	1.04	1.21	0.89	451	0.96	6.93	0.26	2.71	1.75	2.06	ND
37X-1	late Miocene	666.55	4.04	2.76	1.28	0.92	262	0.73	4.42	0.21	2.78	1.46	2.55	ND
42X-3	late Miocene	706.07	2.94	1.66	1.28	1.14	732	1.45	4.69	0.44	1.60	1.54	2.24	ND
46X-6	late Miocene	739.14	3.02	1.77	1.25	1.00	372	1.30	5.18	0.25	2.41	1.86	2.44	ND

Notes: Age = biostratigraphic age (Paull, Matsumoto, Wallace, et al., 1996); C(tot) = total carbon; C(carb) = carbonate carbon [C(tot) – TOC]; TOC = total organic carbon; TS = total sulfur; Sol = solvent-extractable organic matter; Pri = pristane; C17 = n-$C_{17}H_{36}$; Phy = phytane; C18 = n-$C_{18}H_{38}$; OEP 27 = odd-even predominance of n-$C_{27}H_{56}$ vs. (n-$C_{26}H_{54}$ + n-$C_{28}H_{58}$); hop17 = hop17-(21)-ene; hopane = 17α(H),21β(H)-hopane; β,β-hop = 17β(H),21β(H)-hopane; δ13C kerogen = $δ^{12}C/^{13}C$-ratio of kerogen (relative to PDB). ND = no data.
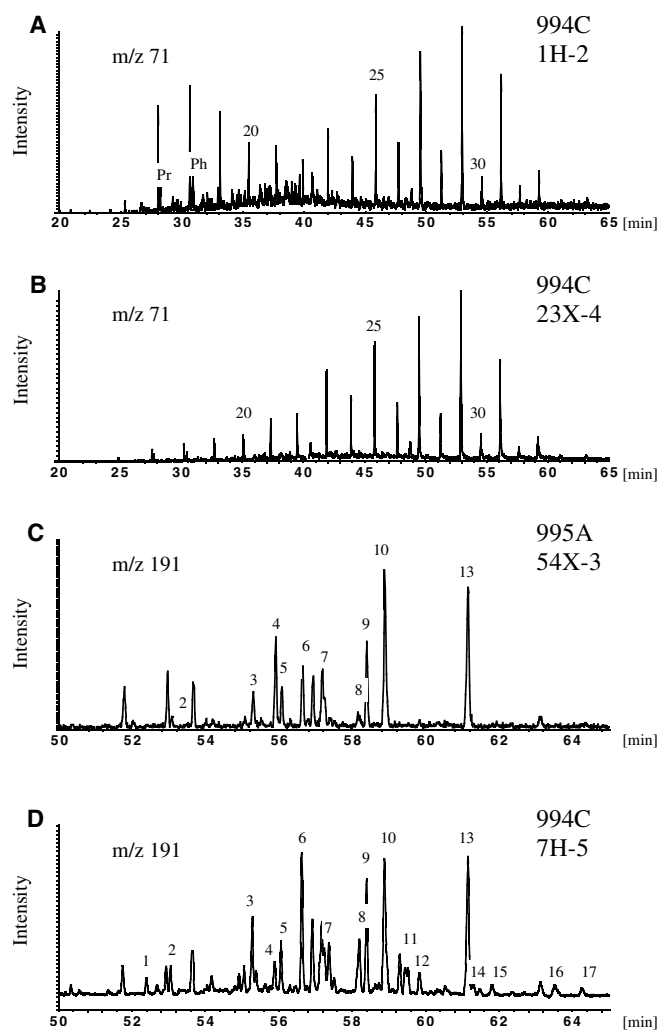
Figure 2. Mass fragmentograms m/z 71 (**A, B**) and m/z 191 (**C, D**) of samples from Holes 994C and 995A. (A) shows algal and higher plant wax contribution, whereas (B) is typical for pure plant wax input. Carbon numbers of the *n*-alkanes and the position of pristane (Pr) and phytane (Ph) are given. (C) shows triterpenoid distributions that are typical for immature organic matter, and the triterpenoid pattern of (D) additionally contains mature compounds (compounds 11–17, except 13). Min = minutes, gas chromatography retention time. For peak identification, see Table 2.

Figure 3. **A.** Pristane/*n*-$C_{17}H_{36}$. **B.** Phytane/*n*-$C_{18}H_{38}$. **C.** Pristane/phytane. **D.** Hop 17-(21)-ene/hopane. **E.** Odd-even predominance (OEP 27, 2* *n*-$C_{27}H_{56}$/ *n*-$C_{26}H_{54}$ + *n*-$C_{28}H_{58}$). **F.** 17ß, 21ß hopane/17α, 21ß hopane vs. depth (mbsf).

several sediment samples from all three holes show an isomerization pattern of the extended hopanes (22S-compound >22R-compound) that is characteristic of mature organic matter (Fig. 2D; Table 2; compounds 11 and 12, 14 and 15, and 16 and 17). The presence of thermally stable and unstable compounds could be due to a mixture of recycled mature and autochthonous immature organic matter (see chapter discussion). However, because all sediments sampled with the grease-containing core barrel have the most pronounced mature pattern, an artificial contamination by grease cannot be excluded. An analysis of the grease in the same way as the samples has yet to be done.

Organic petrographic investigations provide further insight into the composition of the organic matter. In general, the structured organic matter is evenly distributed and not enriched in distinct layers. The particles are around 10 μm in size, and only pollen may exceed 100 μm. Three groups of particles—inertinite, vitrinite (synonymous

with huminite), and liptinite—make up the greater part of the visible organic matter. Bituminite and faunal remains are of minor importance (Table 3). The description of the organic particles visible under the microscope follows the nomenclature of Stach et al., (1982). Submicroscopic organic matter (<1 μm) associated with the inorganic matrix may occur, but it cannot be identified.

1. Inertinite: Highly reflecting inertinite is derived mainly from cell walls of higher plants (mostly trees) and is produced through wildfires. The less-reflecting semi-inertinite is derived from organic matter that has been oxidized in the water column or in the course of early diagenesis. Both constituents are evenly distributed throughout the profiles. Additionally, highly reflective graphite bars, probably derived from eroded crystalline rocks and thin-walled agglomerates, transported as

Table 2. Compounds identified by gas chromatography/mass spectrometry in the saturated hydrocarbon fraction of samples from Holes 994C and 995A.

Number in Figure 2	Compound
1	18α(H)-22,29,30-trisnorneohopane (Ts)
2	17α(H)-22, 29, 30-trisnorhopane (Tm)
3	17α(H),21ß(H)-30-norhopane
4	hop17-(21)-ene
5	17ß(H),21α(H)-30-normoretane
6	17α(H),21ß(H)-hopane
7	17ß(H),21α(H)-moretane
8	17α(H),21ß(H)-homohopane(22S)
9	17α(H),21ß(H)-homohopane(22R)
10	17ß(H),21ß(H)-hopane
11	17α(H),21ß(H)-dihomohopane(22S)
12	17α(H),21ß(H)-dihomohopane(22R)
13	17ß(H),21ß(H)-homohopane
14	17α(H),21ß(H)-trishomohopane(22S)
15	17α(H),21ß(H)-trishomohopane(22R)
16	17α(H),21ß(H)-tetrakishomohopane(22S)
17	17α(H),21ß(H)-tetrakishomohopane(22R)
20	n-$C_{20}H_{42}$
25	n-$C_{25}H_{52}$
30	n-$C_{30}H_{62}$
Pr	Pristane
Phy	Phytane

Note: See Figure 2.

Figure 4. Vitrinite content vs. depth (mbsf) for Holes 994C, 995A, 997A, and 997B.

soot, were observed. Altogether they make up about 50% of the particulate organic matter.

2. Vitrinite: Humic material is also derived from terrestrial vegetation that was degraded during transportation, sedimentation, microbial activity, and inorganic oxidation processes. The particles are fine-grained, elongated, thin-walled, and mostly brown in color. Their concentration is below 5% of total particles in the uppermost samples, whereas it is up to about 50% in the deeper sections.

3. Liptinite: Two major subgroups were differentiated: (1) sporinite, predominantly consisting of saccate pollen from conifers, and (2) alginite, chiefly made up of dinoflagellate cysts and solitary, spiny algae of planktonic origin. Because colonial algae of the Botryococcus type (up to 100 μm in size) are rare, fine-grained liptodetrinite, considered to be algal detritus, is dominating.

These liptinites (pollen and algae) were less degraded than the inertinites and vitrinites.

The composition of the liptinites as a multicomponent group changes downhole. The sporinite dominates, or is in equal concentration to the alginite, in samples down to about 160 mbsf, whereas further down alginite is generally the prevailing constituent of the liptinite.

4. Bituminite: Fluorescing lenses, thin streaks, and agglomerates of bituminite are present in all samples, but only in very small amounts. Some samples contain globular or elliptic brown- to yellow-stained bituminite-like particles, about 10 μm in size, which are interpreted as fecal pellets from copepods and similar crustaceans.

In general, the content of vitrinite increases with depth (Fig. 4), whereas the liptinite content decreases (Table 3). Within the liptinite group, marine algae plays a major role below 180 mbsf, whereas above terrigenous pollen dominate. Taking into account these changes in the composition of the particulate organic matter, with broad scattering the content of marine organic matter (algal-derived) amounts to about 30%, whereas that of terrestrial origin is about 70% in all samples (Table 3).

The maturity of the organic matter, expressed as vitrinite reflectance and measured on only 2–14 particles from each of the six selected samples, is around 0.3%.
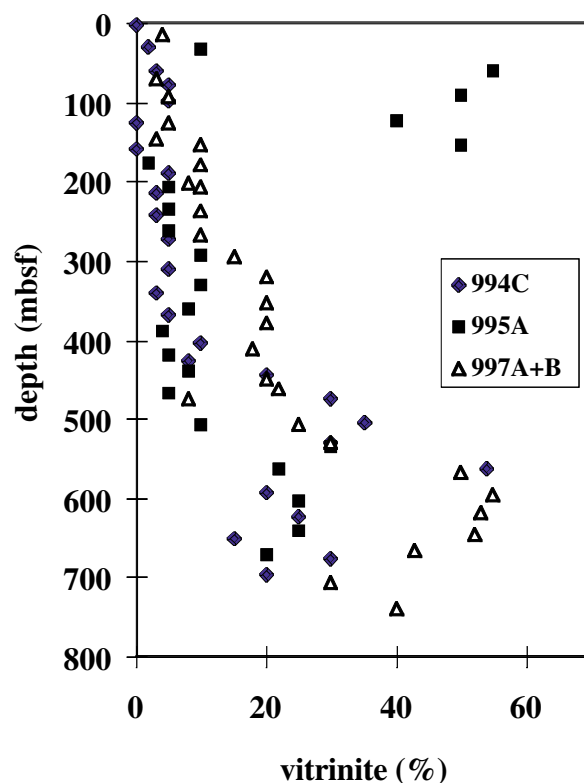
The varying types of organic matter deduced from chemical and optical investigations cannot be verified by the isotope ratios of the kerogens from the Hole 995A (Table 1). $δ^{13}C$ values range between –20.4‰ and –21.9‰, which is generally believed to indicate marine organic matter (Degens, 1969; Kaplan, 1975). On the other hand, a mixture of type II to type III kerogen (Fig. 5) is indicated by the low hydrogen indices (HI; mean HI around 200mg HC/gC) from the shipboard Rock-Eval data (Shipboard Scientific Party, 1996). However, mixed type II/type III organic matter in marine sediments often arises from partial oxidation of type II algal material. Therefore, bulk analysis have to be interpreted with caution.

Amount and Composition of the Combined Gases

The concentrations of the combined gases from Holes 994C, 995A, 997A, and 997B are plotted vs. depth (mbsf) in Figure 6. The data ranges between 73 and 1554 ppbw, 15 and 107 ppbw, and 6 and 61 ppbw for methane, ethane, and propane, respectively. Ethane and propane are constant with depth with the exception of the uppermost samples where the concentrations are slightly increased. Methane is below ≈400 ppbw in the depth range of 200–400 mbsf and below 600 mbsf. Slightly higher methane concentrations are found just above 200 mbsf and between ~450 and 550 mbsf. In the uppermost samples methane values are also slightly higher than below.

The carbon isotope ratios of the combined gases from Holes 994C, 995A, 997A, and 997B are plotted vs. depth in Figure 7. The data ranges between –67‰ and –38‰, –36‰ and –23‰, and –34‰ and –20 ‰ for methane, ethane, and propane, respectively. The isotope data of methane indicates a microbial origin of samples with $δ^{13}C_1 < ≈–55‰$ and a thermal signature for those samples with $δ^{13}C_1 > ≈45‰$. Mixing of methane from different sources or microbial methane oxidation cannot be excluded. Both processes shift the $δ^{13}C_1$ pool towards more positive values. No significant trends in the iso-

Table 3. Organic-petrographical data of samples from Holes 994C, 995A, 997A, and 997B.

Core, section	Depth (mbsf)	1 Liptinite (%)	2 Bituminite (%)	3 Vitrinite (%)	4 Inertinite (%)	5 Spores (%)	6 Algae (%)	7 FP	8 mOM (%)	9 tOM (%)	10 R (%)
164-994C-											
1H-2	2.95	85			15	80	20		17	83	
4H-4	29.35	80		2	18	80	20		16	84	
7H-5	59.35	62		3	35	40	60		37	63	
10H-5	79.35	55		5	40	60	40		22	78	
12H-5	98.35	30		5	65	40	60		18	82	
15H-5	126.13	20			80	40	60		12	88	
20X-1	159.85	15			85	80	20		3	97	
23X-4	189.95	45		5	50	40	60		27	73	
26X-1	214.35	30		3	67	25	75		23	77	
30X-1	243.15	38	P	3	59	20	80		30	70	
33X-2	273.24	10	P	5	85	10	90	P	9	91	
38X-1	310.40	25	P	5	70	10	90		23	77	
41X-2	340.40	30		3	67	10	90		27	73	
44X-2	369.60	40	P	5	55	20	80		32	68	
49X-5	402.62	40	P	10	50	10	90		36	64	
52X-1	425.95	44		8	48	5	95		42	58	
55X-1	444.70	45		20	35		100		45	55	
58X-1	473.90	30	P	30	40	5	95		29	71	
62X-2	504.30	25	P	35	40		100		25	75	
65X-5	529.50	30	1	30	39	5	95		29	71	
69X-3	563.66	15	1	54	30	5	95		14	86	
73X-4	593.07	10		20	70	20	80		8	92	
76X-5	624.30	10		25	65		100		10	90	
79X-4	650.70	30	P	15	55	5	95		29	71	
82X-1	676.05	25	P	30	45	10	90		23	77	
84X-2	696.45	25		20	55	5	95		24	76	
164-995A-											
2H-1	3.15	40			60	35	65		26	74	
5H-1	31.65	30		10	60	45	55		17	83	
8H-2	61.65	15		55	30	25	75		11	89	
12H-3	91.58	25	P	50	25	50	50		12	88	0.33
15H-5	124.15	25		40	35	50	50		12	88	
19H-5	152.78	20		50	30	60	40		8	92	
22X-2	177.60	38	2	2	53	60	40	5	22	78	
25X-3	208.00	25	2	5	68	20	80	P	22	78	
29X-2	235.58	30		5	65	60	40	P	12	88	
32X-1	263.23	35	2	5	58	5	95	P	35	65	
35X-1	291.90	20	P	10	70	40	60	P	12	88	
40X-2	331.64	30	P	10	59	30	70	1	22	78	
43X-2	361.15	15		8	77	50	50	P	8	92	0.32
47X-2	389.85	15	P	4	81	30	70	P	11	89	0.30
51X-2	418.75	15	P	5	80	20	80		12	88	
54X-3	439.60	20	1	8	70	20	80	1	18	82	
57X-2	467.10	15	1	5	79	20	80		13	87	
62X-3	506.56	10	5	10	75	5	95		15	85	
65X-3	536.00	10		30	60	20	80		8	92	
68X-2	563.30	20	4	22	54	35	65		17	83	
73X-4	603.99	15	2	25	58	20	80		14	86	0.29
77X-3	640.27	15	5	25	55	5	95		19	81	
80X-4	671.42	15	5	20	60	5	95		19	81	
164-997A-											
3H-2	15.25	70	2	4	24	30	70	P	51	49	
9H-6	70.35	65		3	32	12	88		57	43	
12H-2	92.70	55		5	40	70	30		17	83	
15H-6	127.35	30		5	65	70	30	P	9	91	
18P-1	146.90	25		3	72	65	35		8	92	
19H-5	154.63	20		10	70	65	35		7	93	
22X-5	179.54	30		10	60	55	45	P	14	86	
25P-1	202.81	20		8	72	40	60	P	12	88	
26X-3	207.85	15	P	10	75	35	65		10	90	
30X-3	236.24	15	2	10	73	35	65		12	88	
34X-4	266.78	15		10	75	20	80	P	12	88	
37X-4	294.85	20	1	15	64	30	70		15	85	
41X-1	320.10	25	3	20	52	30	70	P	20	80	
44X-4	352.60	20		20	60	15	85		17	83	
47X-3	379.67	10	P	20	70	60	40		4	96	
52X-4	411.20	15	2	18	65	20	80		14	86	
164-997B-											
8X-4	448.80	16	4	20	60	20	80		17	83	
10P-1	462.20	12	6	22	60	10	90		17	83	
12X-3	475.56	20	2	8	70	40	60		14	86	
16X-3	506.25	5	P	25	70	50	50		3	97	
19X-1	531.00	10	P	30	60	10	90		9	91	
23X-6	567.35	8	1	50	41	30	70	P	6	94	0.28
27X-5	594.70	12	2	55	31	5	95		13	87	
30X-1	617.50	9	P	53	38	10	90		8	92	
34X-1	646.40	8		52	40	15	85		7	93	0.31
37X-1	666.55	14		43	43	10	90		13	87	
42X-3	706.07	10	1	30	59	5	95		10	90	
46X-6	739.14	10	P	40	50	10	90	P	9	91	

Note: Columns 1 + 2 + 3 + 4 + 7 = 100% structured organic matter; columns 5 + 6 = 100% liptinite; mOM = marine organic matter; tOM = terrestrial organic matter = % vitrinite + % inertinite + (% liptinite × % sporinite/100); FP = fecal pellets; (mOM + tOM) = 100% structured organic matter; R = vitrinite reflectance; P = present.
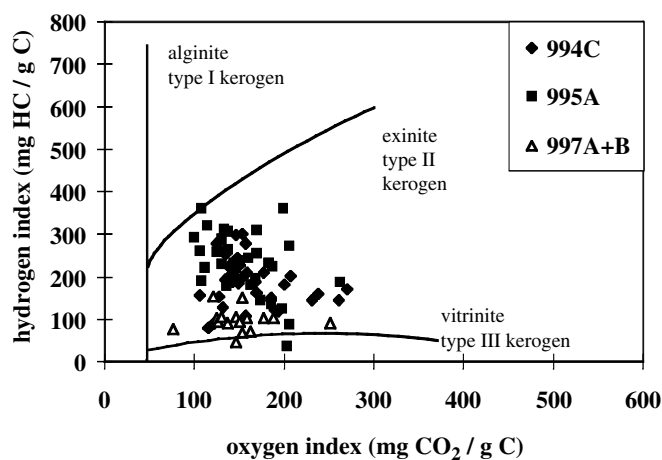
Figure 5. Rock-Eval data (hydrogen index and oxygen index, from Paull, Matsumoto, Wallace, et al., 1996) of samples from Holes 994C, 995A, 997A, and 997B (source of the fields after Simoneit, 1986).

tope data of methane are observed with depth, which could be related to the depth range of the hydrate stability zone. The more positive levels in the upper samples can be explained by microbial oxidation of the free methane that was found in high concentrations above the hydrate stability zone (Paull, Matsumoto, Wallace, et al., 1996). The small trend of the ethane and propane isotope data towards lighter values from bottom to top is difficult to explain genetically. However, because the samples contained large amounts of microbial methane, especially in the upper part of the holes just below the sulfate-reduction zone (Paull, Matsumoto, Wallace, et al., 1996), small amounts of microbial ethane and propane (with $\delta^{13}C_1$ values more negative than −50‰) may also have been formed (Paull et al., Chap. 7, this volume) during methanogenesis. Small amounts of these gases may still be present in the upper samples after ethane- and propane-oxidation and/or after the desorption from the samples ceased. Therefore, the isotope data of ethane and propane may represent a mixture of thermal and, especially in the upper samples, microbial gases.

DISCUSSION

Amount and Type of the Organic Matter

The Leg 164 sediments have TOC values that are typical of ocean margins (1%–2%) and are enriched in organic matter, compared to deep-sea sediments. The reasons might be the additional transport of organic matter from the nearshore environments to the Blake Ridge and enhanced preservation caused by rapid burial. Sedimentation rates increase from about 70 m/m.y. (10^6 yr) within the Quaternary to about 300 m/m.y. within the late Miocene at Site 994 (Paull, Matsumoto, Wallace, et al., 1996). The TOC content follows this increase, at least in the upper part of the profile, down to about 200 mbsf (Fig. 1).

The mass accumulation rate of TOC, which takes into account the porosity and the sedimentation rate of the sediments (van Andel et al., 1975, Stein et al., 1989), increases 25-fold downcore (Fig. 8A) from < 0.02 g cm^{-2} k.y.$^{-1}$ (10^3 yr) in latest Pleistocene to 0.5 g cm^{-2} k.y.$^{-1}$ during the Miocene for sediments from Hole 994C (Paull, Matsumoto, Wallace, et al., 1996). This increase is paralleled by an increase in the vitrinite concentration (Fig. 8B) and by a slight increase of the odd-even predominance of the n-$C_{27}H_{56}$ (Fig. 8C). We believe therefore that the prevalence of the odd-numbered n-alkanes is caused by the presence of terrestrial organic matter and not by marine microalgae (Zegouagh et al., 1998). Both parameters suggest that terrestrial
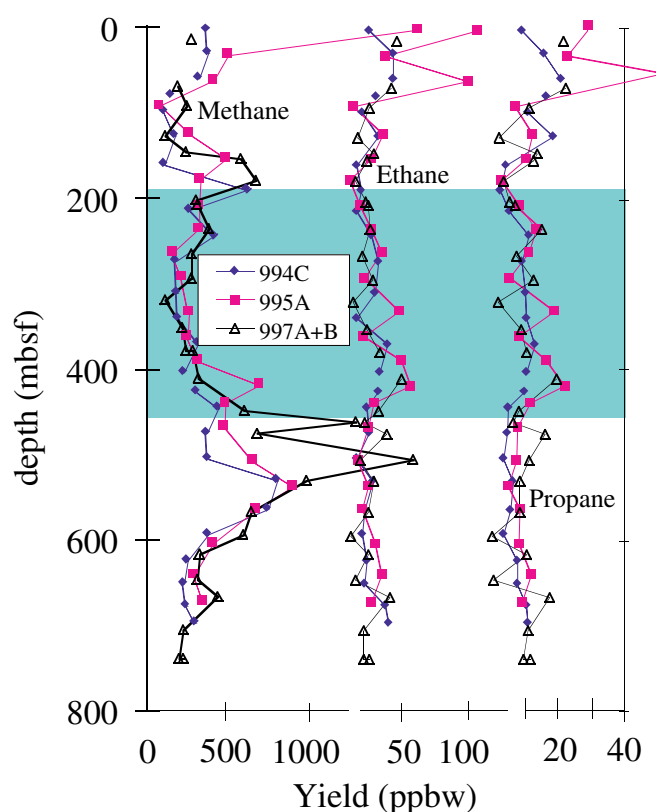
Figure 6. Concentrations of methane, ethane, and propane of the combined gases from Holes 994C, 995A, 997A, and 997B plotted vs. depth (ppbw = parts per billion per weight). Shaded area marks depth range of gas hydrate occurrences, deduced from pore-water chemistry (Paull, Matsumoto, Wallace, et al., 1996).

organic matter occurs more in the older sections. The microscopic investigation of the organic matter, however, reveals a practically constant composition of the particulate organic matter along the profile. A more detailed inspection of the data (Table 3) shows that the organic particles of the uppermost sample from Hole 994C consists of liptinite (85%) and inertinite (15%). The liptinite of this sample is made up of 80% spores (terrigenous) and 20% algae (marine). Therefore, altogether, 17% of the organic particles is of marine and 83% of terrestrial origin. A comparable overall composition was found for the structured organic matter of the lowermost sample from Hole 994C. However, in this case the organic particles consist of only 25% liptinite, which is made up of algae to 95%. Therefore, the marine part of the organic particles amounts to 24% and the terrestrial part to 76%. Additionally, around 20% of the terrigenous organic matter consists of vitrinite, which is not present in the uppermost sample. Obviously, the terms "terrestrial" or "terrigenous," often taken as a synonym for type III kerogen, should be used with caution. It should be kept in mind that sporinite, a liptinite classified as type II kerogen, is of terrestrial origin.

The liptinites (pollen and algae) were less degraded than the inertinites and vitrinites, perhaps because of less transport. It is well established that during transport, deposition, and early diagenesis of organic matter the more stable terrestrially derived compounds will be preserved preferentially (Cornford, 1979). Therefore, the organic matter that has survived and can be analyzed today is only a fraction of the original input, as far as amount and composition is concerned. The observed increase of terrestrially derived organic matter with depth might be due to the preferential removal of more easily degrad-
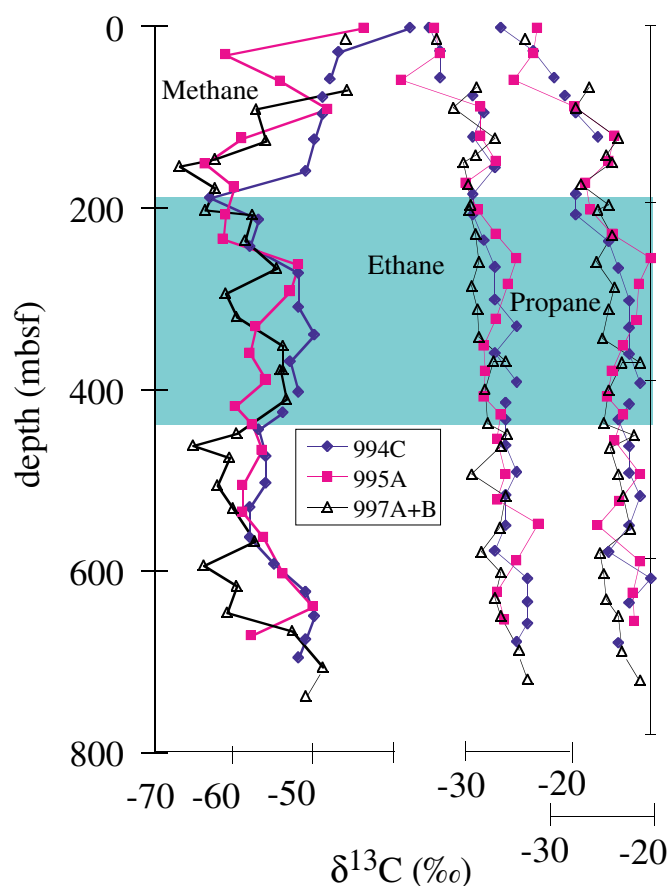
Figure 7. Carbon isotope ratios of methane, ethane, and propane of the combined gases from Holes 994C, 995A, 997A, and 997B plotted vs. depth (mbsf). Shaded area marks depth range of gas hydrate occurrences, deduced from pore-water chemistry (Paull, Matsumoto, Wallace, et al., 1996).

able organic matter of the liptinite group. Therefore, the terrestrially derived organic matter that prevails nowadays in the late Miocene/early Pliocene sediments might be a concentrated residuum. Similar results were achieved by Rullkötter et al. (1986) when looking at Pliocene samples from Hole 533A at the Blake Outer Ridge.

The extractable organic matter of the sediments still contains unsaturated, labile compounds (e.g., hopenes). These compounds are mostly produced through the microbial reworking of the organic matter and do not represent the organic matter input. The increase of the relative concentrations of the microbially produced hopenes and ß,ß-hopanes (Brassell et al., 1981; Ourisson et al., 1984) downhole also may reflect the longer time span available for microbial activity. This may also be true for the increase of the relative isoprenoid concentrations, expressed as phytane/n–$C_{18}H_{38}$ or pristane/phytane ratios.

Hopenes have been found previously in ODP sediments, such as in Pliocene samples off the coast of Chile (Kvenvolden, et al., 1995); however, no clear depth trend was recognized. Kvenvolden et al. (1995) has suggested three possible mechanisms for the observation of C_{32}–C_{35} hopane epimer ratios typical of mature organic matter:

1. Incorporation as recycled material,
2. Migration of hydrocarbons from greater depth, and
3. Mixing of immature and mature components.

However, pollution by grease used for drilling equipment cannot excluded. Further investigations by compound-specific isotope analyses might help to solve this question.
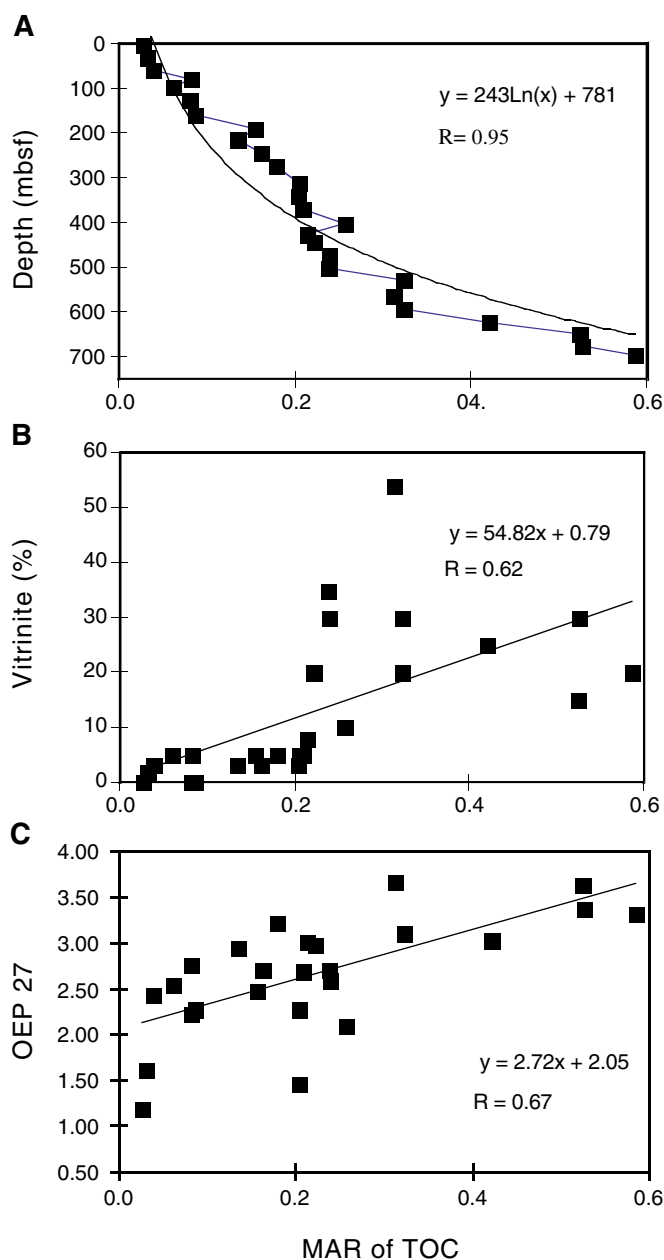
Figure 8. (A) Mass accumulation rate (MAR) of TOC vs. depth, (B) vs. vitrinite concentration, and (C) vs. odd-even predominance (OEP; $2* n\text{-}C_{27}H_{56}/n\text{-}C_{26}H_{54v} + n\text{-}C_{28}H_{58}$). Samples are from Hole 994C.

The hydrogen indices (Espitalié et al., 1985), which range between 100 and 300 mg HC/gC (Paull, Matsumoto, Wallace, et al., 1996), classify the organic matter as a mixture of type II and type III. In detail, samples from Site 997 have somewhat lower HI levels (around 100) than samples from the other two sites, which is reflected by the higher content of inertinite and vitrinite in the Site 997 samples (78%), compared to 67% in Hole 994C samples (Table 3). Selection of organic matter during transport by currents of different intensities on the crest and on the flanks of the ridge might explain this finding. It should be mentioned, however, that only the upper part of the drilled profile of Site 997 has been sampled for Rock-Eval pyrolysis.

There is a discrepancy between the isotopic signature of the kerogen and the facies type of the organic matter that needs further discussion and investigation. The isotope ratios of the kerogens are all

in the range of –21‰ for the Hole 995A samples. This value is often used as an indication for the input of marine plankton that in numerous cases is in the range of –18‰ to –21‰ in Miocene to Holocene sediments (Arthur et al., 1985). However, recent studies of the variation of the $\delta^{13}C$ ratio of modern phytoplankton in different oceanic environments suggest a broader distribution of the $\delta^{13}C$ levels from –21‰ to –8‰ (Popp et al., 1997).

Organic petrographic investigations show the prevalence of inertinite, vitrinite, and sporinite, which are all of terrestrial origin. There are no indications for the occurrence of grasses (C_4 plants), which could be responsible for relatively heavy carbon isotope ratios (Fry et al., 1977). Additionally, the alkane distribution, dominated mostly by n-$C_{29}H_{60}$ (not by n-$C_{31}H_{64}$, which is typical for grasses; Cranwell, 1973), suggests higher land plant (C_3 plants) input, consistent with the Rock-Eval deduced occurrence of type II/III kerogens. Therefore, the kerogen isotope ratios should be in the range of –24‰ to –29‰, typical for the C_3 photosynthetic cycle.

The results of the organic-petrographic investigations and the carbon isotope analyses, which seem to be contradictory at the first glance, might be explained by a mixture of isotopically light terrestrial and isotopically heavy marine organic matter.

Transformation of the Organic Matter in the Sulfate-Reduction Zone

In contrast to the findings of different authors (Vetö et al., 1995; Dean and Arthur, 1989), the hydrogen indices do not correlate with the TOC values. There is also a lack of correlation between TOC and TS content (Berner and Raiswell, 1983). Both observations indicate the degradation of the organic matter that may be used for the sulfate reduction. Another reducing agent besides the sedimentary organic matter could be methane, which migrates in varying amounts from below the sulfate-reduction zone. From the linear shape of the sulfate concentration profile, Borowski et al. (1996) postulated that anaerobic methane oxidation is a major sulfate-consuming process in sediments from the Blake Ridge.

Several authors (Littke et al., 1991; Vetö and Hetényi, 1991; Lallier-Vergès et al., 1993) attempted to quantify the loss of TOC due to microbial sulfate reduction by using the sulfur content of the sediments. This might be possible in nonbioturbated sediments, because the amounts of H_2S that escaped seem to be limited. Stoichiometry shows that 1% reduced sulfur corresponds to a 0.75% loss of TOC (Vetö et al., 1995). However, Blake Ridge sediment bioturbation may result in a substantial loss of H_2S. Therefore, original TOC contents would be higher than calculated by the method of Vetö et al., (1995). On the other hand, if methane is the major organic substrate for the sulfate reduction, the loss would be overestimated.

As a rough estimate and assuming that the loss of H_2S may compensate the nonconsumption of organic matter in the course of sulfate reduction, the concentration of total sulfur is equivalent to the TOC content that might have been lost. Therefore, the original TOC content of the Blake Ridge sediments might have been around 2.5%, in comparison to the mean content of 1.5% today.

Further loss of TOC occurs below the sulfate-reduction zone because of the methane generation. This loss cannot be quantified, because the amount of gas generated is not known. Headspace gas measurements probably give too low of readings because of the loss of gas during core recovery.

Paull et al. (1994) have calculated that under ideal conditions a transformation of 0.5% TOC would be necessary to fill 6% of the pore space with gas hydrate. The pore space of the Blake Ridge sediments from within the gas hydrate–stability zone may be filled up to 9% with hydrates, deduced from direct methane concentration measurements (Dickens et al., 1996) and vertical seismic profiling (Holbrook et al., 1996). These figures are in the same order of magnitude. Therefore, from the quantitative aspect of the available consumable organic matter, the greater part of the methane now occurring as gas

hydrate could be explained as having been generated in situ by microbial activity. The generation might be an ongoing process because viable microbes are present all along the profile (K. Goodman, pers. comm., 1997), as well as metabolizable organic matter (lipids, such as alkanes). However, the carbon isotope ratios of CH_4 and CO_2 of the free gases suggest their migration from depth (Paull et al., Chap. 7, this volume).

Composition of the Combined Gases in Relation to the Gas Hydrate Occurring Zone

No indications of the hydrate-stability zone were found in the concentration data of ethane and propane (Fig. 6) and in the carbon isotope data (Fig. 7). Only minor changes in methane concentrations were observed close to the stability zone, and they are not considered to properly mark the exact depth position of the stability zone in the holes. However, the ratios $C_1/(C_2+C_3)$ plotted vs. depth in Figure 9 are mostly below 10 to 15, somewhat higher in the uppermost samples and significantly higher just above and below the hydrate-stability zone. The reason for the higher levels close to the stability zone is unknown at present, but a possible explanation might be given: gaseous hydrocarbons, of predominantly microbial origin migrate from depth to the surface. The gas hydrate occurring zone (GHOZ) may act as a cap rock, causing an elevated concentration of methane below the seal. Within the GHOZ, part of the methane is densely packed into the hydrate structure, part is filling the pore space as free gas. Thus, an anomalous concentration of methane, which cannot be measured due to the applied sampling technique described in this paper, has to be assumed (Note: the free methane collected with the PCS [Dickens, et al., 1996] has not been considered in this paper). The low methane concentration now observed within the GHOZ is thought to be an artifact, caused by melting of the gas hydrates during core recovery, which is accompanied by a total destruction of the sediment structure ("soupy texture") and a more efficient loss of methane than from over- and underlying horizons.

Higher methane yields above the GHOZ may be caused by the occurrence of hydrates in such a low concentration that their melting did neither influence the pore-water chemistry, nor destroy the sediment structure, but nevertheless contributed to the content of the combined gases. The elevated methane concentrations between ~20 and ~80 mbsf are caused by the active methane generation below the sulfate-reduction zone, which adds additional methane to the stream of migration from below.

Ethane and propane are concentrated relative to methane, which is indicative of thermogenic gases (Fig. 9). The thermal origin of these gases is also evident from their carbon isotope data (Fig. 7), except perhaps for the uppermost samples. Previous investigations of sedimentary gases have shown that data of sorbed gases are hardly influenced by degassing processes (Faber et al., 1990; Whiticar and Suess, 1990; Faber et al., 1997). Therefore, the carbon isotope data from ethane and propane give information on the type and maturity of the corresponding source material. In Figure 10 the carbon isotope data from ethane are crossplotted vs. the propane data. With the exception of the data from the upper parts of the cores, most data points plot along the isotope maturity line shown in Figure 10. This line was constructed according to the model, published by Berner and Faber (1996), for ethane and propane derived from an algal kerogen. It is dependent on the original carbon isotopic composition and the maturity of the kerogen. However, as the sediments from which the gases have been extracted are immature, ethane, propane, and the thermal methane are presumed to have migrated from deeper, more mature parts of the sedimentary column. Assuming the isotopic composition of the kerogen to be $\delta^{13}C = –21$‰, as was determined for kerogens of samples from Hole 995A, then the maturity of the source rock for ethane and propane (Fig. 10) would be in the range between 0.6% to 1.0% vitrinite reflectance (VR). This range corresponds to the oil window maturity stage, the beginning of which was mentioned for
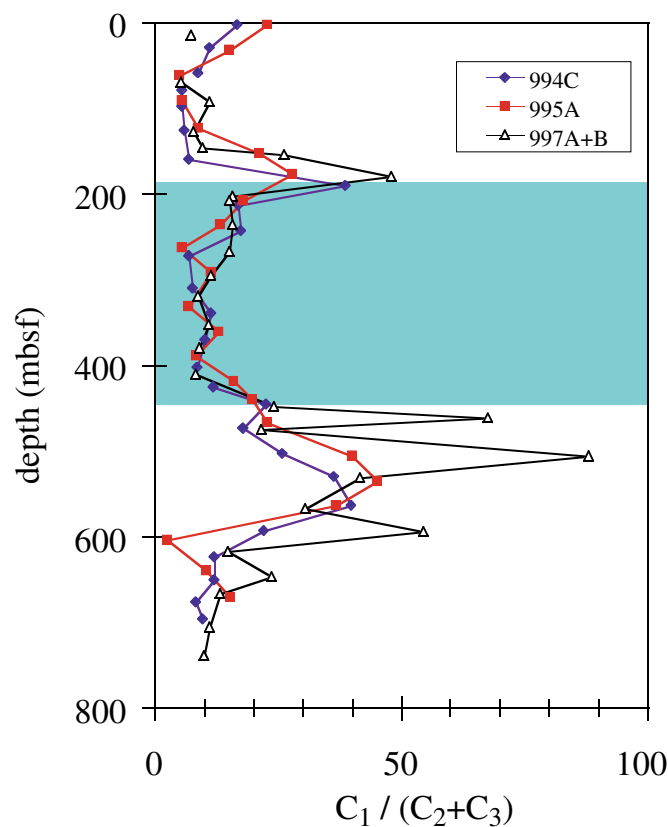
Figure 9. Ratios $C_1/(C_2+C_3)$ of the combined gases from Holes 994C, 995A, 997A, and 997B plotted vs. depth. Shaded area marks depth range of gas hydrate occurrences, deduced from pore-water chemistry (Paull, Matsumoto, Wallace, et al., 1996).

sediments located 1600 m sub-bottom depth (Herbin et al., 1983) at the Blake Bahama Basin close to the survey area.

Mesozoic and Cenozoic formations were drilled during DSDP Legs 44 and 76 within the Blake Bahama Basin. The organic matter from these sediments is mainly of terrestrial origin. However, marine intercalations, equivalents to the Barremian-Cenomanian North Atlantic black shales, have been observed down to 1600 mbsf (Summerhayes and Masran, 1983). The petroleum potential of these horizons, which contain a mixture of detrital and aquatic organic matter, is good to medium, according to Rock-Eval data (Herbin et al.,1983). If similar sediments exist below 1600 mbsf, the higher maturity of the organic matter would be responsible for thermal hydrocarbon generation. Long distance migration, though speculative, may explain the spread of the ethane and propane isotope data.

As mentioned above, the combined methane is a mixture of thermal and microbial contributions and can be characterized according to Figure 11. The data is scattered, as expected for a mixture, but aligns along a mixing line between data of the potential microbial and thermal partners. Because the bulk data in Figure 10 is scattered around 0.8% VR (model: kerogen $\delta^{13}C = -21‰$), the isotope value of the corresponding methane can be calculated to $\delta^{13}C_1 = -36‰$ (according to the model of Berner and Faber, 1996); the corresponding $C_1/(C_2+C_3)$ is 4 (Fig. 11). Assuming $\delta^{13}C_1 = -64‰$ of the residual free methane and $C_1/(C_2+C_3) = 200$ for the sediment gases, the mixing line (Fig. 11) can be fitted to the data. Most of the methane of the combined gases, between 30% and 90%, have a microbial origin. However, the results shown in Figure 11 should not be overinterpreted,

because the combined gases comprise only a small fraction of the originally present total amount of gases, and the concentration of the thermal gases (Fig. 6) is lower by some orders of magnitude than that of the free gases (Paull et al., Chap. 7, this volume). Also, the combined gases may have suffered from microbial (methane) oxidation and desorption from the sediment grains.

CONCLUSIONS

Sediments of Miocene to Pleistocene age were recovered from Holes 994C, 995A, 997A, and 997B, and their gaseous, soluble, and insoluble organic matter contents were investigated. The downhole variations of the amount and composition of the organic matter are virtually parallel in all three holes. The sediments are somewhat enriched in TOC in comparison to most deep-sea sediments. The liptinites are dominated by conifer pollen in the upper sections and by marine algae in the lower ones. Overall, however, an immature terrestrially dominated, mixed type of the particulate organic matter prevails with an increase of the vitrinite with depth. These downhole changes in the organic facies are mirrored by changes in the composition of the soluble organic matter. Its low stage of maturity is confirmed by the occurrence of unsaturated triterpenoids and 17ß, 21ß-pentacyclic triterpenoids.

The organic matter of the drilled sections has a $\delta^{13}C_{org} = -21‰$, which should indicate a prevailing marine facies. However, optical and chemical investigations suggest the prevalence of a mixture of the organic matter: the marine one isotopically heavier, the terrestrial one lighter.

The combined hydrocarbon gases are a mixture of predominantly microbial methane and thermal hydrocarbon gases. Indications of the location of the hydrate stability zone were only found in the data of the gas ratios $C_1/(C_2+C_3)$. Ethane and propane are inferred to have a predominantly thermal origin. On the basis of their carbon isotope ratios and assuming a $\delta^{13}C_{org} = -21‰$, the corresponding source rock should have a marine facies and a maturity in the oil window. Therefore, the bulk of the ethane and propane have migrated from below.

The amount of organic matter that may have been present in the sediments originally would have been sufficient to produce enough methane to fill the pore space to the observed level. An additional supply of methane from deeper sections, however, is inferred from the isotope data.

ACKNOWLEDGMENTS

REFERENCES

Arthur, M. A., Dean, W. E., and Claypool, G. E., 1985. Anomalous ^{13}C enrichment in modern marine organic carbon. *Nature*, 315:216–218.

Berner, U., and Faber, E., 1996. Empirical carbon/isotope maturity relationships for gases from algal kerogens and terrigenous organic matter, based on dry, open-system pyrolysis. *Org. Geochem.*, 24:947–955.

Berner, R.A., and Raiswell, R., 1983. Burial of organic carbon and pyrite sulfur in sediments over Phanerozoic time: a new theory. *Geochim. Cosmochim. Acta,* 47:855–862.

Blumer, M., Guillard, R.R.L., and Chase, T., 1971. Hydrocarbons of marine phytoplankton. *Mar. Biol.,* 8:183–189.

Borowski, W.S., Paull, C.K., and Ussler, W., III, 1996. Marine pore-water sulfate profiles indicate in situ methane flux from underlying gas hydrate. *Geology,* 24:655–658.

Brassell, S.C., Wardroper, A.M.K., Thomson, I.D., Maxwell, J.R., and Eglinton, G., 1981. Specific acyclic isoprenoids as biological markers of methanogenic bacteria in marine sediments. *Nature,* 290:693–696.

Claypool, G.E., Presley, B.J., and Kaplan, I.R., 1973. Gas analyses in sediment samples from Legs 10, 11, 13, 14, 15, 18, and 19. *In* Creager, J.S., Scholl, D.W., et al., *Init. Repts. DSDP,* 19: Washington (U.S. Govt. Printing Office), 879–884.

Cornford, C., 1979. Organic deposition at a continental rise: organic geochemical interpretation and synthesis at DSDP Site 397, Eastern North Atlantic. *In* von Rad, U., Ryan, W.B.F., et al., *Init.Repts. DSDP,* 47 (Pt. 1): Washington (U.S. Govt. Printing Office), 503–510.

Cranwell, P. A., 1973. Chain-length distribution of n-alkanes from lake sediments in relation to post-glacial environmental change. *Freshwater Biol.,* 3:259–265.

Dean, W.E., and Arthur, M.A., 1989. Iron-sulfur-carbon relationships in organic-carbon-rich sequences, I. Cretaceous western interior seaway. *Am. J. Sci.,* 289:708–743.

Degens, E.T., 1969. Biogeochemistry of stable carbon isotopes. *In* Eglinton, G., and Murphy, M.T.J. (Eds.), *Organic Geochemistry:* Berlin (Springer-Verlag), 304–329.

Dickens, G.R., Wallace, P., and Paull, C.K., 1996. In-situ methane quantities across a bottom simulating reflector on the Blake Ridge. *1st MASTER Wkshp. Gas Hydrates,* Gent, Belgium, 14–15. (Abstract)

Dumke, I., Faber, E., and Poggenburg, J., 1989. Determination of stable carbon and hydrogen isotopes of light hydrocarbons. *Anal. Chem.,* 61:2149–2154.

Eglinton, G., and Hamilton, R.J., 1963. The distribution of alkanes. *In* Swain, T. (Ed.), *Chemical Plant Taxonomy:* London (Academic Press), 187–208.

Espitalié, J., Deroo, G., and Marquis, F., 1985. La pyrolyse Rock-Eval et ses applications, Partie I. *Rev. Inst. Fr. Pet.,* 40/5:563–579.

Faber, E., Berner, U., Hollerbach, A., and Gerling, P., 1997. Isotope geochemistry in surface exploration for hydrocarbons. *Geol. Jahrb.,* 103:103–127.

Faber, E., and Stahl, W., 1983. Analytical procedure and results of an isotope geochemical surface survey in an area of the British North Sea. *In* Brooks, J. (Ed.), *Petroleum Geochemistry and Exploration of Europe.* Geol. Soc. Spec. Publ. London, 12:51–63.

Faber, E., Stahl, W.J., Whiticar, M.J., Lietz, J., and Brooks, J.M., 1990. Thermal hydrocarbons in Gulf Coast sediments. *GCSSEPM Found. Ninth Ann. Res. Conf. Proc.,* 297–307.

Fry, B., Scalan, R.S., and Parker, P.L., 1977. Stable carbon isotope evidence for two sources of organic matter in coastal sediments: seagrasses and plankton. *Geochim. Cosmochim Acta,* 41:1875–1877.

Herbin, J.P., Deroo, G., and Roucaché, J., 1983. Organic geochemistry in the Mesozoic and Cenozoic formations of Site 534, Leg 76, Blake Bahama Basin, and comparison with Site 391, Leg 44. *In* Sheridan, R.E., and Gradstein, F.M., et al., *Init. Repts. DSDP,* 76: Washington (U.S. Govt. Printing Office), 481–493.

Holbrook, W.S., Hoskins, H., Wood, W.T., Stephen, R.A., Lizzarralde, D., and the Leg 164 Science Party, 1996. Methane gas-hydrate and free gas on the Blake Ridge from vertical seismic profiling. *Science,* 273:1840–1843.

Hufnagel, H., and Porth, H., 1989. Organopetrographic studies in the Visayan Basin, Philippines. *Geol. Jahrb.,* 70:349-384.

Kaplan, I.R., 1975. Stable isotopes as a guide to biogeochemical processes. *Proc. R. Soc. London B,* 189:183–211.

Kvenvolden, K.A., and Barnard, L.A., 1983. Gas hydrates of the Blake Outer Ridge, Site 533, Deep Sea Drilling Project Leg 76. *In* Sheridan, R.E., Gradstein, F.M., et al., *Init. Repts. DSDP,* 76: Washington (U.S. Govt. Printing Office), 353–365.

Kvenvolden, K.A., Rullkötter, J., Hostettler, F.D., Rapp, J.B., Littke, R., Disko, U., and Scholz-Böttcher, B., 1995. High-molecular-weight hydrocarbons in a south latitude setting off the coast of Chile, Site 859. *In* Lewis, S.D., Behrmann, J.H., Musgrave, R.J., and Cande, S.C. (Eds.), *Proc. ODP, Sci. Results,* 141: College Station, TX (Ocean Drilling Program), 287–297.

Lallier-Vergès, E., Bertrand, P., Huc, Y., Bückel, D., and Tremblay, P., 1993. Control of preservation of organic matter by productivity and sulphate reduction in Kimmeridgian shales from Dorset (UK). *Mar. Pet. Geol.,* 10:600–605.

Littke, R., Baker, D.R., Leythaeuser, D., and Rullkötter, J., 1991. Keys to the depositional history of the Posidonia Shale (Toarcian) in the Hils Syncline, northern Germany. *In* Tyson, R.V., and Pearson, T.H. (Eds.), *Modern and Ancient Continental Shelf Anoxia.* Geol. Soc. Spec. Publ. London, 58:311–333.

Ourisson, G., Albrecht, P., and Rohmer, M., 1984. The microbial origin of fossil fuels. *Sci. Am.* 251:44–51.

Paull, C.K., Matsumoto, R., Wallace, P.J., et al., 1996. *Proc. ODP, Init. Repts.,* 164: College Station, TX (Ocean Drilling Program).

Paull, C.K., Ussler, W., III, and Borowski, W.A., 1994. Sources of biogenic methane to form marine gas-hydrates: in situ production or upward migration? *Ann. N.Y. Acad. Sci.,* 715:392–409.

Popp, B.N., Parekh, P., Tilbrook, B., Bidigare, R.R. and Laws, E.A., 1997. Organic carbon $\delta^{13}C$ variations in sedimentary rocks as chemostratigraphic and paleoenvironmental tools. *Palaeogeogr., Palaeoclimatol., Palaeoecol.,* 132:119-132.

Rullkötter, J., Mukhopadhyay, P.K., Disko, U., Schaefer, R.G., and Welte, D.H., 1986. Facies and diagenesis of organic matter in deep sea sediments from the Blake Outer Ridge and the Blake Bahama Basin, Western North Atlantic. *Mitt. Geol.-Palaeontol. Inst. Univ. Hamburg,* 60:179-203.

Sheridan, R.E., Gradstein, F.M., et al., 1983. *Init. Repts. DSDP,* 76: Washington (U.S. Govt. Printing Office).

Shipboard Scientific Party, 1972. Sites 102-103-104—Blake-Bahama Outer Ridge (northern end). *In* Hollister, C.D., Ewing, J.I., et al., *Init. Repts. DSDP,* 11: Washington (U.S. Govt. Printing Office), 135–218.

Shipboard Scientific Party, 1996. Explanatory notes. *In* Paull, C. K., Matsumoto, R., Wallace, P. J., et al., *Proc. ODP, Init. Repts.,* 164: College Station, TX (Ocean Drilling Program), 13-41.

Simoneit, B.R.T., 1986. Organic geochemistry of black shales from the Deep Sea Drilling Project, a summary of the occurrences from the Pleistocene to the Jurassic. *Mitt. Geol.-Palaeontol. Inst. Univ. Hamburg,* 60:275-309.

Stach, E., Mackowsky, M.-T., Teichmüller, M., Taylor, G.H., Chandra, D., and Teichmüller, R., 1982. *Stach's Textbook of Coal Petrology* (3rd ed.): Berlin (Gebrüder Borntraeger).

Stein, R., ten Haven, H.L., Littke, R., Rullkötter, J., and Welte, D.H., 1989. Accumulation of marine and terrigenous organic carbon at upwelling Site 658 and nonupwelling Sites 657 and 659: implications for the reconstruction of paleoenvironments in the eastern subtropical Atlantic through late Cenozoic times. *In* Ruddiman, W., Sarnthein, M., et al., *Proc. ODP, Sci. Results,* 108: College Station, TX (Ocean Drilling Program), 361–385.

Summerhayes, C.P., and Masran, T.C., 1983. Organic facies of Cretaceous and Jurassic sediments from Deep Sea Drilling Project Site 534 in the Blake Bahama Basin, Western North Atlantic. *In* Sheridan, R.E., and Gradstein, F.M., et al., *Init. Repts. DSDP,* 76: Washington (U.S. Govt. Printing Office), 469–480.

van Andel, T.H., Heath, G.R., and Moore, T.C., Jr., 1975. Cenozoic history and paleoceanography of the central equatorial Pacific Ocean: a regional synthesis of Deep Sea Drilling Project data. *Mem.—Geol. Soc. Am.,* 143.

Vetö, I., and Hetényi, M., 1991. Fate of organic carbon and reduced sulphur in dysoxic-anoxic Oligocene facies of the Central Paratethys (Carpathian Mountains and Hungary). *Geol. Soc. Spec. Publ. London,* 50:449-460.

Vetö, I., Hetényi, M., Demény, A., and Hertelendi, E., 1995. Hydrogen index as reflecting intensity of sulphidic diagenesis in non-bioturbated, shaly sediments. *Org. Geochem.,* 22:299–310.

Whiticar, M.J., and Suess, E., 1990. Characterization of sorbed volatile hydrocarbons from the Peru margin, Leg 112, Sites 679, 680/681, 682, 684, and 686/687. *In* Suess, E., von Huene, R., et al., *Proc. ODP, Sci. Results,* 112: College Station, TX (Ocean Drilling Program), 527–538.

Zegouagh, Y., Derenne, S., Largeau, C., Bardoux, G., and Mariott, A., 1998. Organic matter sources and early diagenetic alterations in Arctic surface sediments (Lena River delta and Laptev sea, Eastern Siberia), II. Molecular and isotopic studies of hydrocarbons. *Org. Geochem.,* 28:571-583.
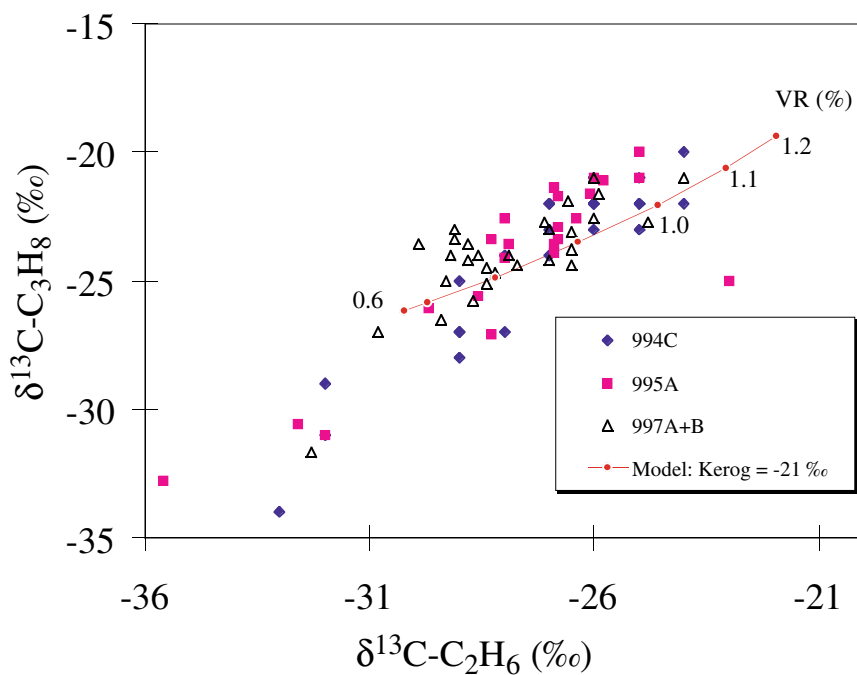
Figure 10. Carbon isotope data of ethane and propane from the combined gases compared to isotope/maturity relationships for marine kerogens, derived after the model from Berner and Faber (1996).
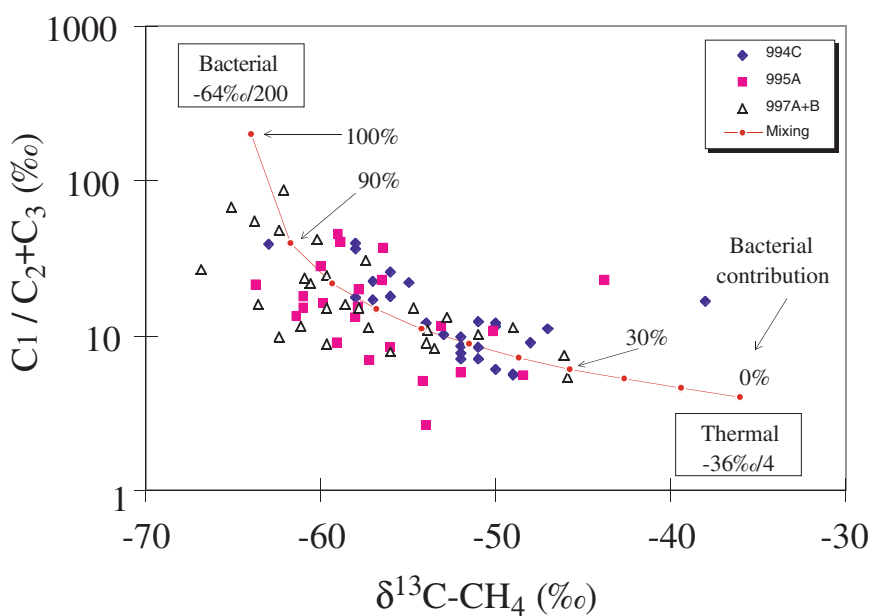
Figure 11. Carbon isotope data of methane and the C_1/(C_2+C_3) ratio of the combined gases from Holes 994C, 995A, 997A, and 997B. The microbial proportion of the methane is indicated by the numbers (in percent) at the calculated mixing line.